Direct Antenna Frequency-Hopped M-FSK Modulation With Time-Modulated Arrays

Roberto Maneiro-Catoira [ID], *Member, IEEE*, Julio Brégains [ID], *Senior Member, IEEE*, José A. García-Naya [ID], *Senior Member, IEEE*, and Luis Castedo [ID], *Senior Member, IEEE*

Abstract—We present an innovative approach that simultaneously enables direct antenna frequency-hopped M-ary frequency shift keying (DAFH-MFSK) modulation and beamsteering through the use of time-modulated arrays (TMAs). The distinctive feature of our approach lies in the modulation of the TMA excitations with binary periodic sequences, which can be easily frequency-adjusted and time-delayed to simultaneously allow for DAFH-MFSK direct antenna modulation and beamsteering. Notably, our TMA proposal offers a distinct advantage over conventional architectures in terms of performance metrics, including reduced insertion losses and enhanced phase resolution for beamsteering, while also simplifying hardware complexity.

Index Terms—Beamsteering (BS), direct antenna modulation (DAM), frequency hopping, frequency shift keying modulation, time-modulated arrays.

I. INTRODUCTION

LOW-POWER and low-data-rate Internet of Things (IoT) wireless devices widely use frequency-shift keying (FSK) modulation due to their simplicity and resilience to noise and attenuation [1]. In standard M-ary FSK (MFSK) [2, Ch. 5], a constant-amplitude sine carrier with frequency $f_c + f_{FSK}^m = f_c + m\Delta f_{FSK}$, $m \in \mathcal{M} = \{1, 2, \ldots, M\}$ is selected every symbol period T_s, depending on which symbol is to be transmitted, being f_c the reference (or base) carrier frequency, and Δf_{FSK} the separation between two adjacent f_{FSK}^m values. Accordingly, $B_{FSK} = M\Delta f_{FSK}$ corresponds to the total FSK bandwidth.

Despite their advantages, MFSK signals can be easily intercepted and, moreover, can be seriously distorted by frequency selective channels. These drawbacks can be overcome by means of frequency-hopping (FH) techniques [2, Ch. 13], which randomly change the carrier frequency in every hop period T_h. We assume hopping frequencies that are randomly selected from a set of equally spaced frequencies $f_{FH}^k = (k-1)\Delta f_{FH}$, $k \in \mathcal{K} = \{1, 2, \ldots, K\}$ with Δf_{FH} being
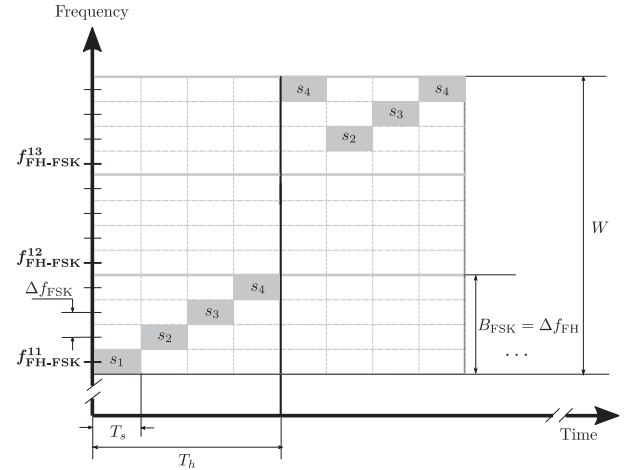
Fig. 1. Time-frequency diagram for slow FH-FSK modulation with $M = 4$, $K = 3$, and $L = 4$. The transmitted MFSK symbols are denoted by s_m, $m \in \mathcal{M}$.

the separation between any two adjacent f_{FH}^k. We consider $\Delta f_{FH} = M\Delta f_{FSK}$, hence the transmit frequency for every T_s in FH-FSK is $f_{FH\text{-}FSK}^{mk} = f_c + f_{FSK}^m + f_{FH}^k = f_c + [m + (k-1)M]\Delta f_{FSK}$, whereas $W = K\Delta f_{FH} = KB_{FSK}$ is the total transmission bandwidth. We focus on slow FH where $T_h = LT_s$ ($L \in \mathbb{N}$), as shown in Fig. 1, which contains the time-frequency plot of an FH-FSK transmission. Since demodulation requires knowledge of the pseudorandom FH pattern, FH-FSK prevents eavesdropping while increases robustness to frequency-selective channels.

Another concept, in line with IoT, is direct antenna modulation (DAM), which consists in modulating the carrier in the antenna itself [3], [4]. DAM replaces baseband modulation and significantly reduces transmission hardware (HW) complexity, cost, and power consumption [5], [6], [7]. Furthermore, since modulation occurs after amplification, power amplifiers (PAs) only need to amplify a single carrier, hence avoiding wideband PAs.

This letter combines FH-FSK and DAM into a transmission method termed DAFH-MFSK and proposes an innovative approach for its implementation using a highly efficient and versatile single sideband (SSB)[1] TMA [8], [9], [10], [11], [12], [13] which, in addition, is capable of performing beamsteering (BS).

[1]Single sideband (SSB) TMAs remove unwanted frequency-mirrored beam patterns produced by conventional TMAs to achieve high efficiency levels.
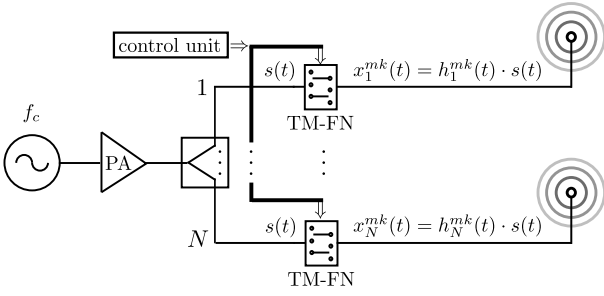
Fig. 2. Proposed time-modulated array (TMA) architecture to jointly perform direct antenna frequency-hopped M-ary frequency shift keying (DAFH-MFSK) modulation and BS. The schematic of a time-modulating feeding network (TM-FN) module is detailed in Fig. 3(b). For each modulating waveform $h_n^{mk}(t)$, $n \in \mathcal{N}$ denotes the corresponding antenna element, $m \in \mathcal{M}$ is the FSK symbol transmitted, and $k \in \mathcal{K}$ is the hop frequency slot. In the text, the values of m and k will be single digits so that the notation with the superscript mk is not misleading.

II. JOINT DAFH-MFSK MODULATION AND BS: A TMA APPROACH

A. SSB Time Modulating Feeding Network

Fig. 2 plots the proposed SSB TMA architecture for DAFH-MFSK, equipped with periodic time-modulating feeding networks (TM-FNs) to jointly perform DAFH-MFSK modulation and BS. We consider a linear array of N isotropic elements with unitary static excitations, $I_n = 1$, $n \in \mathcal{N}$, and $\mathcal{N} = \{1, \ldots, N\}$. The nth element excitation is modulated during a symbol period T_s by the periodic pulsed signal $h_n^{mk}(t)$, which is a time-shifted version of the stair-step approximation to $h^{mk}(t)$ [see Fig. 3(a)], an LP-TM waveform [12] with unit amplitude and phase varying from 0 to $5\pi/3$ (six steps). Therefore, $h_n^{mk}(t) = h^{mk}(t - D_n^{mk})$, being D_n^{mk} a variable time-delay. Notice that $h_n^{mk}(t)$ has a fundamental period $T_{\mathrm{TMA}}^{mk} = 1/f_{\mathrm{TMA}}^{mk} \ll T_s$, where $m \in \mathcal{M}$ refers to the transmitted mth FSK-modulated level, and $k \in \mathcal{K}$ accounts for the hop frequency slot selected during T_s.

The synthesis of $h_n^{mk}(t)$ is described using a switched TM-FN [see Fig. 3(b)]. Considering the rectangular pulse signal $p^{mk}(t) = 1$ when $0 \leq t < T_{\mathrm{TMA}}^{mk}/6$, and $p^{mk}(t) = 0$; otherwise, we can express a single period of $h^{mk}(t)$ as $\sum_{l=0}^{5} p^{mk}(t - \frac{l T_{\mathrm{TMA}}^{mk}}{6}) e^{j\frac{2\pi l}{6}}$. Hence, the exponential Fourier series coefficients of the periodic signal $h^{mk}(t)$ are

$$H_q^{mk} = \begin{cases} \frac{6}{\pi q} \sin\left(\frac{\pi q}{6}\right) e^{j\frac{\pi q}{6}}, & q \in \Psi \\ 0, & q \notin \Psi; \Psi = \{q = 6i+1; i \in \mathbb{Z}\}. \end{cases} \tag{1}$$

The Fourier coefficients H_q^{mk} are the same for all values of m and k because $h^{mk}(t)$ is always a time-scaled version of the waveform shown in Fig. 3(a). In view of (1), the Fourier coefficients of $h_n^{mk}(t) = h^{mk}(t - D_n^{mk})$ are given by

$$H_{nq}^{mk} = \begin{cases} H_q^{mk} e^{-j2\pi q f_{\mathrm{TMA}}^{mk} D_n^{mk}}, & q \in \Psi \\ 0, & q \notin \Psi \end{cases} \tag{2}$$

and the exponential Fourier series expansion of $h_n^{mk}(t)$ is

$$h_n^{mk}(t) = \sum_{q \in \Psi} H_q^{mk} e^{-j2\pi q f_{\mathrm{TMA}}^{mk} D_n^{mk}} e^{j2\pi q f_{\mathrm{TMA}}^{mk} t}. \tag{3}$$

According to (2), Fig. 4 shows the normalized Fourier series power spectrum of $h_n^{mk}(t)$ in dB, namely, $20 \log_{10} |H_{nq}^{mk}/H_{n1}^{mk}|$. We can see, apart from the SSB property of the waveform, that the most meaningful unwanted harmonic is the one with order $q = -5$, whose relative level is at -13.97 dB with respect to the useful harmonic $q = 1$.

TMA periodic modulating signals, $h_n^{mk}(t)$, have the following features.
1) They have no frequency-mirrored harmonics (hence the term SSB) and their first positive harmonic concentrates almost all the transmitted energy.
2) This harmonic is located at $f_{\mathrm{TMA}}^{mk} = f_{\mathrm{FH}}^{k} + f_{\mathrm{FSK}}^{m}$, hence the TMA transmits the mth level within the kth FH slot.
3) The phase term of the first positive Fourier coefficient of $h_n^{mk}(t)$ is proportional to the time delay D_n^{mk} [see (2)], which is instrumental to determine the steering direction of the TMA beampattern and, unlike digital variable phase shifters (VPSs) in standard phased arrays, D_n^{mk} can be adjusted almost continuously [11], [14].

In addition to the rejection threshold of unwanted harmonics shown in Fig. 4, the time-modulation efficiency of the TMA is $\eta_{\mathrm{TM}} = \mathcal{P}_U^{\mathrm{TM}}/\mathcal{P}_R^{\mathrm{TM}}$, where $\mathcal{P}_U^{\mathrm{TM}}$ and $\mathcal{P}_R^{\mathrm{TM}}$ are the respective useful and total average power radiated by the TMA. According to [15, Eq. 16], η_{TM} is given by

$$\eta_{\mathrm{TM}} = \left|H_{n1}^{mk}\right|^2 / \sum_{q \in \Psi} \left|H_{nq}^{mk}\right|^2. \tag{4}$$

Since $h_n^{mk}(t)$ has unit amplitude, then

$$\frac{1}{T_{\mathrm{TMA}}^{mk}} \int_0^{T_{\mathrm{TMA}}^{mk}} |h_n^{mk}(t)|^2 dt = \sum_{q \in \Psi} |H_{nq}^{mk}|^2 = 1 \tag{5}$$

thus obtaining [see (2) and (4)]

$$\eta_{\mathrm{TM}} = |H_{n1}^{mk}|^2 = [6/\pi \cdot \sin(\pi/6)]^2 = 0.912. \tag{6}$$

This means that the proposed SSB TMA architecture ensures that more than 91 % of the total energy is transmitted over the first positive harmonic. On the basis of this result, the following approximation is applicable in (3)

$$h_n^{mk}(t) \approx H_1^{mk} e^{-j2\pi f_{\mathrm{TMA}}^{mk} D_n^{mk}} e^{j2\pi f_{\mathrm{TMA}}^{mk} t}. \tag{7}$$

B. Signal Radiated During a Symbol Period

As shown in Fig. 2, the input to the proposed SSB TMA is the single-frequency carrier signal $s(t) = e^{j2\pi f_c t}$. During a symbol period T_s, the TMA excitations are time modulated by $h_n^{mk}(t)$ and the signal radiated by the TMA in the spatial direction θ is given by

$$x^{mk}(\theta, t) = \sum_{n=1}^{N} h_n^{mk}(t) e^{j\beta_c z_n \sin\theta} s(t) \tag{8}$$

where z_n is the position of the nth array element on the z-axis and $\beta_c = 2\pi/\lambda_c$ is the wavenumber for a carrier wavelength $\lambda_c = c/f_c$. Normalizing (7) with respect to H_1^{mk}, which is the same for all values of m and k [see (1)], (8) can be rewritten as

$$x^{mk}(\theta, t) \approx \sum_{n=1}^{N} e^{j2\pi\left(\frac{z_n}{\lambda_c}\sin\theta - f_{\mathrm{TMA}}^{mk} D_n^{mk}\right)} e^{j2\pi\left(f_c + f_{\mathrm{TMA}}^{mk}\right)t}$$

$$\approx \underbrace{\mathrm{AF}^{mk}(\theta)}_{\mathrm{BS}} \cdot \underbrace{e^{j2\pi f_{\mathrm{FH\text{-}FSK}}^{mk} t}}_{\mathrm{DAFH\text{-}MFSK\ modulation}} \tag{9}$$
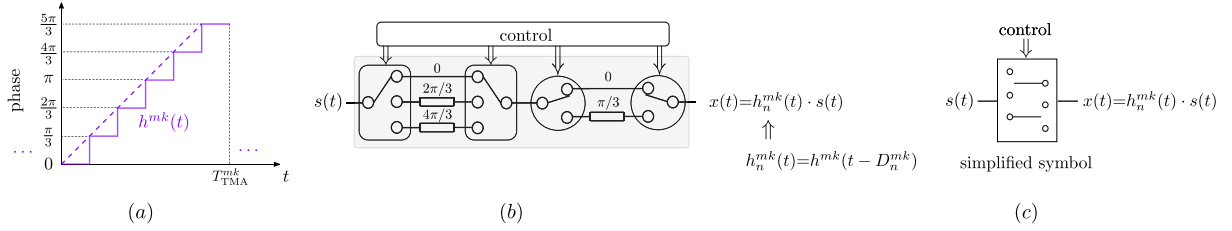
Fig. 3. (a) Periodical (T_{TMA}^{mk}) six-level linear-phase time-modulating (LP-TM) signal, which allows for the direct transmission of the mth FSK symbol over the kth FH slot using a TMA. Notice that only $\angle h^{mk}(t)$ is sketched since $|h^{mk}(t)| = 1 \; \forall m, k$. To additionally perform BS, in the nth antenna element, $h^{mk}(t)$ is subject to a time-delay D_n^{mk}, i.e., $h_n^{mk}(t) = h^{mk}(t - D_n^{mk})$. (b) Switched TM-FN of the nth TMA element, which consists of two single-pole triple-throw (SP3T) switches and two single-pole dual-throw (SPDT) switches or, equivalently, six SPDT switches, to time modulate an input signal $s(t)$ with $h_n^{mk}(t)$; and (c) simplified block diagram of (b).
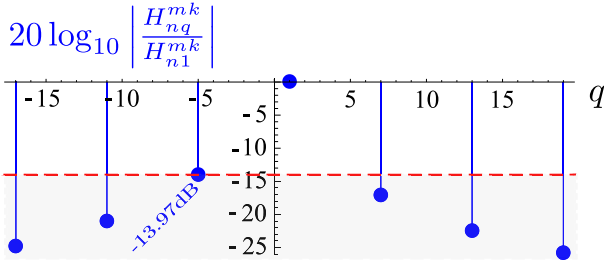

Fig. 4. Normalized Fourier series power spectrum of $h_n^{mk}(t)$. All unwanted harmonics have a minimum rejection level of 13.97 dB with respect to the exploited harmonic at $q = 1$. Notice that $|H_{nq}^{mk}|$ is the same for all values of m, k, and n for a given q because $h_n^{mk}(t)$ is either a time-scaled version (when m and/or k changes) or a time-shifted version (when n changes) of the same waveform.

where the term $\text{AF}^{mk}(\theta) = \sum_{n=1}^{N} \mathrm{e}^{\mathrm{j}2\pi(\frac{z_n}{\lambda_c}\sin\theta - f_{\text{TMA}}^{mk}D_n^{mk})}$ is the spatial array factor during T_s and provides the BS ability to the TMA. Indeed, the maximum of the radiation pattern can be pointed to the direction θ_0 by adjusting the delays D_n^{mk}, $n \in \mathcal{N}$, so that the following equation is satisfied:

$$\mathrm{e}^{\mathrm{j}2\pi f_{\text{TMA}}^{mk}D_n^{mk}} = \mathrm{e}^{\mathrm{j}2\pi\frac{z_n}{\lambda_c}\sin\theta_0} \tag{10}$$

in which case the array factor is

$$\text{AF}^{mk}(\theta) = \sum_{n=1}^{N} \mathrm{e}^{\mathrm{j}2\pi\frac{z_n}{\lambda_c}(\sin\theta - \sin\theta_0)}. \tag{11}$$

On the other hand, the term $\mathrm{e}^{\mathrm{j}2\pi f_{\text{FH-FSK}}^{mk}t}$ in (9) allows the TMA to transmit the mth FSK level over the kth FH slot, and thus perform DAFH-MFSK modulation.

III. CASE STUDY AND COMPARATIVE ANALYSIS

This section has a twofold purpose: 1) demonstrate the feasibility of the proposed technique by means of numerical simulations, and (2) compare it with conventional architectures performing FH-MFSK and BS simultaneously.

A. Numerical Example

Let us consider a DAFH-MFSK modulator architecture based on TM-FNs (refer to Fig. 2). We assume the following parameters: carrier frequency: $f_c = 2.5$ GHz; number of antenna elements: $N = 4$, spaced $\lambda_c/2$ apart; modulation scheme: 4-FSK ($M = 4$); hopping frequencies: 6 possible values ($K = 6$); symbol period: $T_s = 10$ ms; hop duration: $L = 4$, thus

TABLE I
FREQUENCIES AND TIME DELAYS D_n^{m2} (NANOSECONDS) OF THE TMA MODULATING WAVEFORMS FOR THE HOP FREQUENCY $f_{\text{FH}}^2 = 200$ kHz AND THE FOUR 4-FSK LEVELS $m = \{1, 2, 3, 4\}$ TO STEER THE BEAM TOWARDS $\theta_0 = 30°$ (SEE FIG. 5)

m	$f_{\text{FSK}}^m + f_{\text{FH}}^2$	D_1^{m2}	D_2^{m2}	D_3^{m2}	D_4^{m2}
1	250 kHz	500	1000	1500	2000
2	300 kHz	417	833	1250	1667
3	350 kHz	357	714	1071	1429
4	400 kHz	313	625	938	1250

$T_h = 4T_s = 4$ ms; frequency separation for FSK: $\Delta f_{\text{FSK}} = 50$ kHz, with $f_{\text{FSK}}^1 = 50$ kHz; and frequency spacing for FH: $\Delta f_{\text{FH}} = 200$ kHz, with $f_{\text{FH}}^1 = 0$ Hz. The minimum frequency of the TMA modulating waveforms is given by $f_{\text{TMA}}^{11} = f_{\text{FH}}^1 + f_{\text{FSK}}^1 = 50$ kHz, corresponding to their maximum possible period $T_{\text{TMA}}^{\max} = T_{\text{TMA}}^{11} = 1/f_{\text{TMA}}^{11} = 20\mu\text{s} \ll T_s = 10$ ms. In addition, the TMA offers a minimum period of $T_{\text{TMA}}^{\min} = T_{\text{TMA}}^{46} = 1/f_{\text{TMA}}^{46} = 833$ ns.

As an example, let us consider that the TMA radiates sequentially the four 4-FSK levels $m = \{1, 2, 3, 4\}$ over the second ($k = 2$) FH slot of duration T_h and centered at frequency $f_{\text{FH}}^2 = f_{\text{FH}}^1 + \Delta f_{\text{FH}} = 250$ kHz. The frequencies to be transmitted and the antenna elements time delays D_n^{m2}, $n \in \mathcal{N}$, [determined according to (10)] to point the maximum of the radiation pattern towards $\theta_0 = 30°$ are shown in Fig. 5 and summarized in Table I.

B. Comparison With Conventional Techniques

Fig. 6 shows the block diagram of a conventional FH-MFSK transmitter followed by a standard phased array equipped with digitally tuned passive VPSs to perform BS. Every T_s, the incoming binary data bits are employed, via a multiplexer (MUX), to select the transmitting carrier frequency from a pool of M possibilities. The FH-MFSK signal is generated by mixing the resulting MFSK modulated signal with a carrier obtained from a digital frequency synthesizer under the control of a code generator.

Given that the mixer produces both sum and difference frequency components, but only the sum frequency is intended for radiation, a bandpass filter (BPF) is placed after the mixer. Following amplification through the PA, the signal is radiated to a given direction by adjusting the VPSs within the standard phased array.
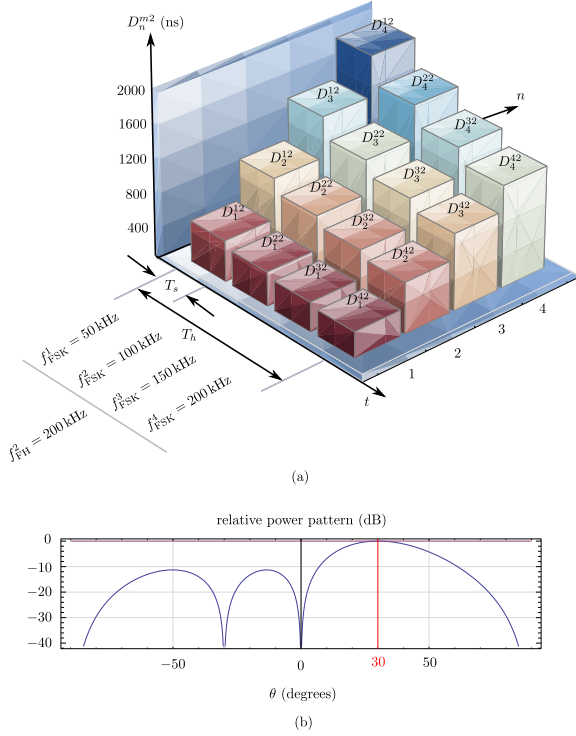
(a)

(b)

Fig. 5. (a) Time delays D_n^{m2} specified in Table I as a function of $n \in \mathcal{N}$ and time. During T_h, the sequence of symbols s_m, corresponding to the frequencies f_{FSK}^m, $m = \{1, 2, 3, 4\}$, are transmitted. (b) Relative power radiated pattern of the proposed TMA. When its modulating waveforms are subject to D_n^{m2} during the considered T_h, the beampattern points towards $\theta_0 = 30°$.
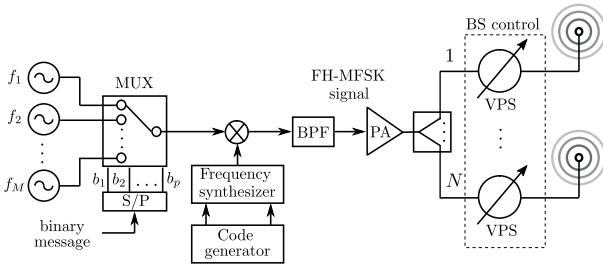

Fig. 6. Block diagram of a conventional FH-MFSK transmitter followed by a standard phased array with digitally tuned passive VPS to perform BS.

Compared with the conventional scheme in Fig. 6, our proposed TMA approach in Fig. 2 offers several key advantages as follows.

1) *Reduced HW complexity:* In our approach, there is no need for a MUX, mixer, frequency synthesizer, or BPF, and the PA only needs to amplify a single carrier.

2) *Minimal oscillator requirements:* Unlike the conventional scheme illustrated in Fig. 6, which necessitates multiple oscillators corresponding to the number of MFSK levels, M, our approach requires just one oscillator. Refer to Table II where we employ big O notation [16] for a comprehensive HW comparison.

3) *Reduced number of SPDT switches:* The number of SPDT swtches in our approach is only half that of the conventional scheme employing 6-bit VPSs (minimum resolution comparable to that of the TMA [11]). This results in a linear complexity, as detailed in Table II.
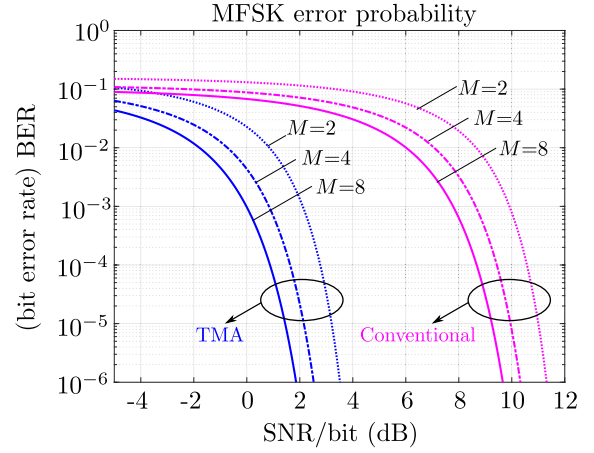

Fig. 7. Performance of MFSK demodulation for the proposed TMA approach (see Fig. 2) and the conventional one (see Fig. 6) in terms of BER versus received SNR per bit in the conventional scheme.

TABLE II
COMPARATIVE ADVANTAGES OF THE PROPOSED TMA APPROACH

FH-MFSK and BS Scheme	# Oscillators	# SPDT switches	η (dB)
Conventional (Fig. 6)	$M \in O(M)$	$12N \in O(N)$	11.2
This work: TMA approach (Fig. 2)	$1 \in O(1)$	$6N \in O(N)$	3.4

4) *Improved insertion losses:* For both the conventional architecture and the TMA approach, we consider off-the-shelf devices with the lowest insertion loss, denoted as η, within the specified frequency band. Specifically, $\eta_{\text{MUX}} = 0.7$ dB [single-pole four-throw (SP4T) switch] [17], $\eta_{\text{mixer}} = 4.5$ dB [18], $\eta_{\text{BPF}} = 2$ dB [19], $\eta_{\text{VPS}} = 4$ dB [17], $\eta_{\text{SPDT}} = 0.5$ dB [17], and ideal $1{:}N$ power splitters are taken into account.

Under these circumstances, the conventional architecture exhibits an insertion loss of $\eta_{\text{conv}} = \eta_{\text{MUX}} + \eta_{\text{mixer}} + \eta_{\text{BPF}} + \eta_{\text{VPS}} = 11.2$ dB. In contrast, the TMA approach [20] demonstrates significantly lower insertion losses, with $\eta_{\text{TMA}} = -10 \log_{10} \eta_{\text{TM}} + 6\eta_{\text{SPDT}} = 3.4$ dB. Consequently, assuming equal power levels in the respective carrier signals, the same PA gain, and that the performance of all components remains consistent across the entire bandwidth, the proposed TMA approach achieves a substantial insertion loss reduction of $\Delta\eta = \eta_{\text{TMA}} - \eta_{\text{conv}} = -7.8$ dB. This insertion loss reduction leads to a significant performance improvement of MFSK demodulation in terms of bit error ratio (BER) versus received signal-to-noise ratio (SNR) per bit, as illustrated in Fig. 7.

IV. CONCLUSION

We have introduced an innovative TMA approach that seamlessly combines DAFH-MFSK modulation and BS, making it particularly well suited for low-power and low-data-rate applications. This approach offers several key advantages over comparable existing architectures, including better energy efficiency, simplified design, and the ability to achieve continuous phase-sensitivity BS.

REFERENCES

[1] "Keysight application notes." Accessed: Mar. 3, 2023. [Online]. Available:https://www.keysight.com/us/en/assets/7018-03097/application-notes/5990-8818.pdf

[2] A. Goldsmith, *Wireless Communications*. Cambridge, U.K.: Cambridge Univ. Press, 2005.

[3] V. Fusco and Q. Chen, "Direct-signal modulation using a silicon microstrip patch antenna," *IEEE Trans. Antennas Propag.*, vol. 47, no. 6, pp. 1025–1028, Jun. 1999.

[4] S. Keller, W. Palmer, and W. Joines, "Direct antenna modulation: Analysis, design, and experiment," in *Proc. IEEE Antennas Propag. Soc. Int. Symp.*, 2006, pp. 909–912.

[5] S. Henthorn, K. L. Ford, and T. O'Farrell, "Bit-error-rate performance of quadrature modulation transmission using reconfigurable frequency selective surfaces," *IEEE Antennas Wireless Propag. Lett.*, vol. 16, pp. 2038–2041, 2017.

[6] S. Henthorn, K. L. Ford, and T. O'Farrell, "Direct antenna modulation for high-order phase shift keying," *IEEE Trans. Antennas Propag.*, vol. 68, no. 1, pp. 111–120, Jan. 2020.

[7] P. James and R. G. Nair, "A study on adaptive direct antenna modulation," in *Proc. Int. Conf. Emerg. Technological Trends*, 2016, pp. 1–6.

[8] P. Rocca, G. Oliveri, R. J. Mailloux, and A. Massa, "Unconventional phased array architectures and design methodologies–A review," *Proc. IEEE*, vol. 104, no. 3, pp. 544–560, Mar. 2016.

[9] R. Maneiro-Catoira, J. Brégains, J. A. García-Naya, and L. Castedo, "Time-modulated array beamforming with periodic stair-step pulses," *Signal Process.*, vol. 166, 2020, Art. no. 107247.

[10] R. Maneiro-Catoira, J. Brégains, J. A. García-Naya, and L. Castedo, "Time-modulated phased array controlled with nonideal bipolar squared periodic sequences," *IEEE Antennas Wireless Propag. Lett.*, vol. 18, no. 2, pp. 407–411, Feb. 2019.

[11] Q. Chen, J.-D. Zhang, W. Wu, and D.-G. Fang, "Enhanced single-sideband time-modulated phased array with lower sideband level and loss," *IEEE Trans. Antennas Propag.*, vol. 68, no. 1, pp. 275–286, Jan. 2020.

[12] G. Ni, C. He, Y. Gao, J. Chen, and R. Jin, "High-efficiency modulation and harmonic beam scanning in time modulated array," *IEEE Trans. Antennas Propag.*, vol. 71, no. 1, pp. 368–380, Jan. 2023.

[13] E. Aksoy and E. Afacan, "Calculation of sideband power radiation in time-modulated arrays with asymmetrically positioned pulses," *IEEE Antennas Wireless Propag. Lett.*, vol. 11, pp. 133–136, 2012.

[14] Q. Zeng et al., "Phase modulation technique for harmonic beamforming in time-modulated arrays," *IEEE Trans. Antennas Propag.*, vol. 70, no. 3, pp. 1976–1988, Mar. 2022.

[15] R. Maneiro Catoira, J. Brégains, J. A. Garcia-Naya, L. Castedo, P. Rocca, and L. Poli, "Performance analysis of time-modulated arrays for the angle diversity reception of digital linear modulated signals," *IEEE J. Sel. Topics Signal Process.*, vol. 11, no. 2, pp. 247–258, Mar. 2017.

[16] T. H. Cormen, C. E. Leiserson, R. L. Rivest, and C. Stein, *Introduction to Algorithms*, 4th ed., Cambridge, MA, USA: MIT Press, 2001.

[17] Analog Devices, "SPDT switches. HMC284 A, SP4T switches. HMC241AQ516, VPS HMC647 A." Accessed: Jan. 9, 2023. [Online]. Available: https://www.analog.com

[18] Marki Microwave, "Mixer basics primer.," Accessed: Sep. 24, 2023. [Online]. Available: https://markimicrowave.com/technical-resources/white-papers/mixer-basics-primer/

[19] Minicircuits, "Band pass filters: BFCN-2435." Accessed: Sep. 24, 2023. [Online]. Available: http://www.minicircuits.com

[20] R. Maneiro-Catoira, J. A. García-Naya, J. C. Brégains, and L. Castedo, "Multibeam single-sideband time-modulated arrays," *IEEE Access*, vol. 8, pp. 151976–151989, 2020.